

We are IntechOpen, the world's leading publisher of Open Access books Built by scientists, for scientists

6,900

Open access books available

186,000

International authors and editors

200M

Downloads

Our authors are among the

154

Countries delivered to

TOP 1%

most cited scientists

12.2%

Contributors from top 500 universities



WEB OF SCIENCE™

Selection of our books indexed in the Book Citation Index
in Web of Science™ Core Collection (BKCI)

Interested in publishing with us?
Contact book.department@intechopen.com

Numbers displayed above are based on latest data collected.
For more information visit www.intechopen.com



Optical Detection of Protein Adsorption on Doped Titanium Surface

Raimo Silvennoinen et al.*

*Department of Physics and Mathematics, University of Eastern Finland, Joensuu
Finland*

1. Introduction

The frequently used biomaterial in hard tissue replacement, such as dental and orthopaedic implants, is titanium. (Ball et al., 1996; Höök et al., 2002a; Huang et al., 2003; Imamura et al., 2008; Jones et al., 2000; Walivaara et al., 1994; Yang et al., 2003) These kind of biomaterial applications made of titanium are satisfactory products, because of their ability to adsorb certain proteins. After implantation, within a few seconds, the biomaterial surface becomes coated with a film of adsorbed proteins mediating the interaction between the implant and the body environment. Since an implant is exposed to blood during implantation, the initial protein layer is mainly composed of plasma proteins. Human plasma fibrinogen (HPF) is the relevant protein, which adsorbs on biomaterial surfaces. HPF partakes in blood coagulation, facilitates adhesion and aggregation of platelets (Cacciafesta et al., 2001; 2000). The structure and composition of the adsorbed protein layer determine the type and extent of the subsequent biological reactions, such as activation of coagulation and immune response and osseointegration (Nygren et al., 1997). Thus, the initially adsorbed protein layer is a factor determining the biocompatibility (Cai et al., 2006; Galli et al., 2001; Garguilo et al., 2004; Hemmersam et al., 2005; Kidoaki & Matsuda, 1999; Ma et al., 2007; Rouahi et al., 2006; Van De Keere et al., 2008; Wang et al., 2003), and also in recent years interest has been focused to preparation of hydrocarbons doped with Ti and used different methods to analyzing of biocompatibility for important proteins (Choukourov et al., 2008; Grinevich et al., 2009; Silvennoinen, Hason, Vetterl, Penttinen, Silvennoinen, Myller, Cernochova, Bartakova, Prachar & Cvrcek, 2010; Silvennoinen, Vetterl, Hason, Tuononen, Silvennoinen, Myller, Cvrcek, Vanek & Prachar, 2008).

The production and application of doped titanium surfaces are under intensive research, and the results have shown the positive views on the adaptation of these materials as a biomaterial, as equal or even better than the bulk titanium. The doping of titanium is performed typically by inserting impurities like N, Nb, Zr, Ta, Al, Cr and V, into the titanium crystal structure. (Archana et al., 2010; Barajas-Ledesma et al., 2010; Cantau et al., 2010; Choi et al., 2010; Czoska et al., 2011; Darriba et al., 2009; Huang et al., 2010; Khaleel et al., 2010; Martin et al., 2006; Shaama, 2005)

*Niko Penttinen, Martti Silvennoinen (*Department of Physics and Mathematics, University of Eastern Finland, Joensuu, Finland*), Stanislav Hason, Vladimír Vetterl (*Institute of Biophysics, v.v.i., Academy of Science of the Czech Republic, Brno, Czech Republic*), Sonia Bartáková, Patrik Prachár, Jiří Vaněk, Vítězslav Březina (*Centre for Dental and Craniofacial Research, Faculty of Medicine, Masaryk University, Brno, Czech Republic*)

Substantial progress has been made in understanding adhesion process on surfaces after or while immersed in liquids. In these research a number of developed techniques such as, X-ray photoelectron spectroscopy (XPS), atomic force microscopy (AFM), ellipsometry, fourier transform infrared attenuated total reflectance (FTIR/ATR), quartz crystal microbalance (QCM), surface plasmon resonance (SPR), dual polarization interferometry, total internal reflectance fluorescence (TIRF), voltammetry and electrochemical impedance spectroscopy (EIS) have been deployed. When measuring in liquid environment the potential amount of usable devices rapidly decreases and none of the listed devices are alone able to describe, in detail, the adsorption process of biomolecules. (Agnihotri & Siedlecki, 2004; Cacciafesta et al., 2001; Cai et al., 2006; 2005; Höök et al., 2002b; Jackson et al., 2000; Jandt, 2001; Roach et al., 2005; Roach, Farrar & Perry, 2006; Roach, Shirtcliffe, Farrar & Perry, 2006; Soman et al., 2008; Sonesson et al., 2007; Swann et al., 2004; Toscano & Santore, 2006; Van De Keere et al., 2008; Vanderah et al., 2004; Wang et al., 2003; Wertz & Santore, 1999; 2001; 2002; Xu & Siedlecki, 2007)

Adsorption of HPF molecules at the rough bulk titanium and modified titanium surfaces increases the scattering and decreases the coherence of the probing laser light beam. These changes in coherence as well as in signal magnitude can be detected with diffractive optical element (DOE) based sensor. DOE sensor is a non-contact optical method, in detection of biomolecules, which can sense changes on the measured biosurface as well as changes in the surface itself. (Silvennoinen, Hason, Vetterl, Penttinen, Silvennoinen, Myller, Cernochova, Bartakova, Prachar & Cvrcek, 2010; Silvennoinen, Peiponen & Myller, 2008; Silvennoinen, Vetterl, Hason, Silvennoinen, Myller, Vanek & Cvrcek, 2010; Silvennoinen, Vetterl, Hason, Tuononen, Silvennoinen, Myller, Cvrcek, Vanek & Prachar, 2008)

HPF protein molecules adsorb stronger on the titanium surface, which is treated by polishing and etching, than at the surface treated only by polishing due to an increase of surface area caused by etching and thus increase the interactions caused by van der Waals forces (Parsegian, 2005; Silvennoinen, Hason, Vetterl, Penttinen, Silvennoinen, Myller, Cernochova, Bartakova, Prachar & Cvrcek, 2010; Silvennoinen, Vetterl, Hason, Tuononen, Silvennoinen, Myller, Cvrcek, Vanek & Prachar, 2008). The effective surface tension, as well as the surface energy related to the topography of surface, is assumed to influence the final interactions of the implant with the surrounding environment. It is also reported that rough surfaces promote better osseointegration than smooth surfaces (Brett et al., 2004; Cochran, 1999; Jansson & Tengvall, 2004; Webster et al., 1999).

Treatment of titanium surface by titanium doped hydrocarbon layer is observed to have strong influence on the adsorption of HPF molecules. Also HPF adsorption is detected on the titanium alloy surface as Ti6Al4V. Adsorption of the elongated HPF on a titanium-based surface is monitored by analyzing permittivity and optical roughness of protein-modified surfaces by using a DOE sensor and a variable angle spectro-ellipsometry (VASE). The biological experiment, when cultivation of osteoblast at the titanium surface was performed, showed that the surface treated by polishing and etching is more proper for the bone cell growth than the surface treated only by polishing. The best adsorption of fibrinogen was observed at the titanium doped hydrocarbon surface prepared by plasma-enhanced chemical vapor deposition, when the optimal ratio was $Ti_{0.38}C_{0.62}$ and $Ti_{0.09}C_{0.91}$. The surface of dental implants treated by this way should increase their biocompatibility, speed up their osseointegration and healing. Also, due to low value of Young modulus and relatively easy forming, even in cold processing, the alloys could be the future material in implantology.

Aging of titanium surface affects to the adsorption behavior of HPF proteins, which may be caused from the consecutive adsorption of carbon and oxygen from air on the surface

during the long-term storage of bulk biomaterial. Aging showed decreases in the adhesion magnitudes of titanium doped hydrocarbon surfaces after long term storage, caused by the surface reacting with molecules of air (Silvennoinen, Vetterl, Hason, Tuononen, Silvennoinen, Myller, Cvrcek, Vanek & Prachar, 2008).

2. Characterization of surface

2.1 Diamond stylus

Diamond stylus is one of the standardized and classical methods in measuring the surface roughness. The idea of stylus profilometer is that a thin stylus (with diameter only few microns) is scanned on the measured surface along a line. When a small force is applied to the stylus, the vertical movement can be measured revealing the hills and valleys of the surface ie. the real surface topography. In figure 1 is shown a surface profile measured from a non-polished Si(100) surface.

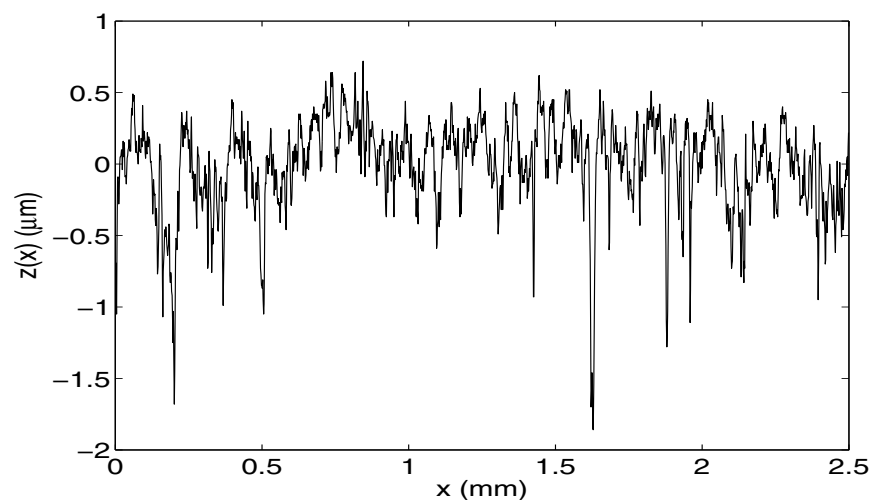


Fig. 1. The measured surface profile $z(x)$ as a function of stylus scan length x . For this surface $R_a = 0.23 \mu\text{m}$, $R_q = 0.31 \mu\text{m}$ and R_z (peak to valley value) = $2.44 \mu\text{m}$.

When the profile curve is recorded, one can calculate various roughness parameters, like average surface as follows

$$R_a = \frac{1}{L} \int_0^L |z(x) - \langle z(x) \rangle| dx, \quad (1)$$

where the stylus scan length is L , x is the position along the scan length, $z(x)$ is the vertical position of stylus as a function of x , brackets ($\langle \rangle$) denote the mean value with minimum variance and vertical bar brackets ($| |$) denote the absolute value. Another often used parameter is root-mean-square (rms) surface roughness, which can be expressed

$$R_q = \sqrt{\frac{1}{L} \int_0^L (z(x) - \langle z(x) \rangle)^2 dx}. \quad (2)$$

In general the $R_a \leq R_q$.

2.2 Spectral ellipsometry (VASE)

Spectral ellipsometer can be considered as a special reflectometer, where the only difference is the polarization state of the reflected light wavefront measured from sample surface. The analysis of reflected wavefront data is performed by using the Fresnel laws to solve the optical parameters related to surface such as complex refractive index ($N = n + i\kappa$, where i denotes imaginary unit). The amplitude reflection coefficient (r) of the TM- and TE-polarized light at the angle of incidence (θ_i) can be expressed with the following equations

$$r_{\text{TM}} = \frac{(n_2 - i\kappa_2)^2 \cos\theta_i - n_1 \sqrt{(n_2 - i\kappa_2)^2 - n_1^2 \sin^2\theta_i}}{(n_2 - i\kappa_2)^2 \cos\theta_i + n_1 \sqrt{(n_2 - i\kappa_2)^2 - n_1^2 \sin^2\theta_i}} \quad (3)$$

and

$$r_{\text{TE}} = \frac{n_1 \cos\theta_i - \sqrt{(n_2 - i\kappa_2)^2 - n_1^2 \sin^2\theta_i}}{n_1 \cos\theta_i + \sqrt{(n_2 - i\kappa_2)^2 - n_1^2 \sin^2\theta_i}}, \quad (4)$$

where n_1 denotes the refractive index of air and $N_2 = n_2 + i\kappa_2$ is the complex refractive index of the reflective material. The respective reflectances for the TM- and TE-polarized light are as follows

$$R_{\text{TM}} = r_{\text{TM}} r_{\text{TM}}^* \quad \text{and} \quad R_{\text{TE}} = r_{\text{TE}} r_{\text{TE}}^*, \quad (5)$$

where the asterisk denotes the complex conjugate. The complex ratio of the amplitude reflectances ($r_{\text{TM}}/r_{\text{TE}}$) can be expressed as follows

$$\frac{r_{\text{TM}}}{r_{\text{TE}}} = \tan\Psi e^{i\Delta}, \quad (6)$$

where $\tan\Psi$ is the amplitude part and $i\Delta$ is the phase part of propagating complex amplitude. Right side of the equation 6 is assumed to be in a form which can be measured experimentally. Utilizing the equation 6, the complex refractive index can be calculated at a known wavelength which was used to measure Ψ and Δ . Example of measured spectral refractive index is presented in figure 2 from vacuum evaporated gold (Au) film surface.

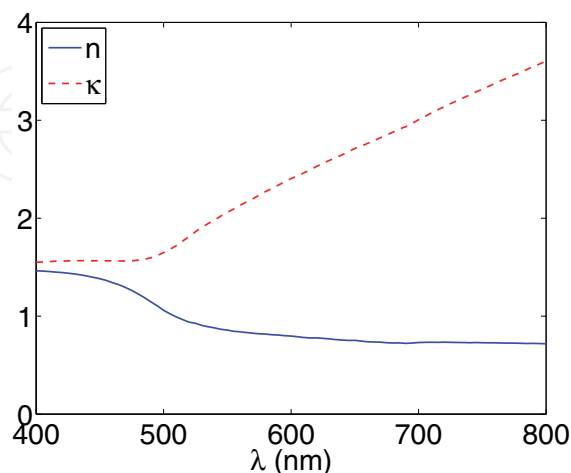


Fig. 2. Measured spectral n and κ ($N = n + i\kappa$) of a gold (Au) film surface measured with VASE.

2.3 Gloss and optical roughness by DOE

DOE sensors have been proven to be accurate in sensing optical changes in two main surface properties as permittivity and roughness also in nanometer scale. Specular reflectance is a function of three variables: complex refractive index/permittivity, angle of incident of the probe beam and surface topography. Standardized specular gloss (G) relates to reflectance and it is normalized to the reflectance of black glass having gloss value of 100 gloss units (GU). The optical roughness, which relates to the surface topography, is sensed as optical path differences which the rough surface generates in reflection. In DOE sensor measurements; (I) the probe beams angle of incidence remains constant (perpendicular to the surface), (II) the complex refractive index of the measured surface is known (measured) and (III) the surface topography acts as a variable. Before DOE measurements, the spectral complex refractive index (N) of each material surface is characterized with variable angle spectro-ellipsometer (VASE). General principle of DOE is to focus coherent light to a 4×4 dot matrix, which takes the optimal shape in its focal plane at wanted wavelength. The formed DOE image is then detected with CCD-camera and saved into personal computers (PC) memory for further analysis (Fig. 3).

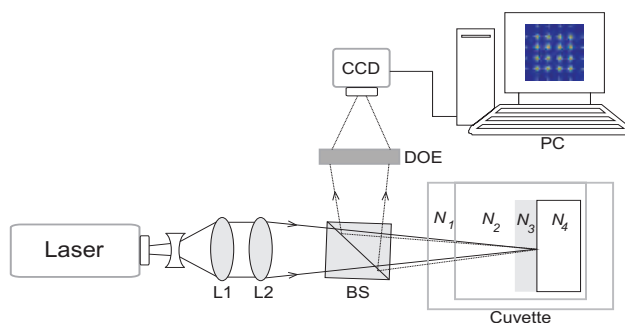


Fig. 3. DOE sensor setup with lenses L1 and L2, beam splitter (BS), sample cuvette, CCD camera, refractive indexes N_1 - N_4 and personal computer (PC) for analyzing. DOE image with the 4×4 dot matrix is shown on the screen of PC.

In figures 4 and 5 are presented the gloss and R_{opt} maps scanned from a polished titanium (Ti_p) surface with $20 \mu\text{m}$ probe beam waist diameter. Scanning was done in air from $2\text{mm} \times 2\text{mm}$ surface area.

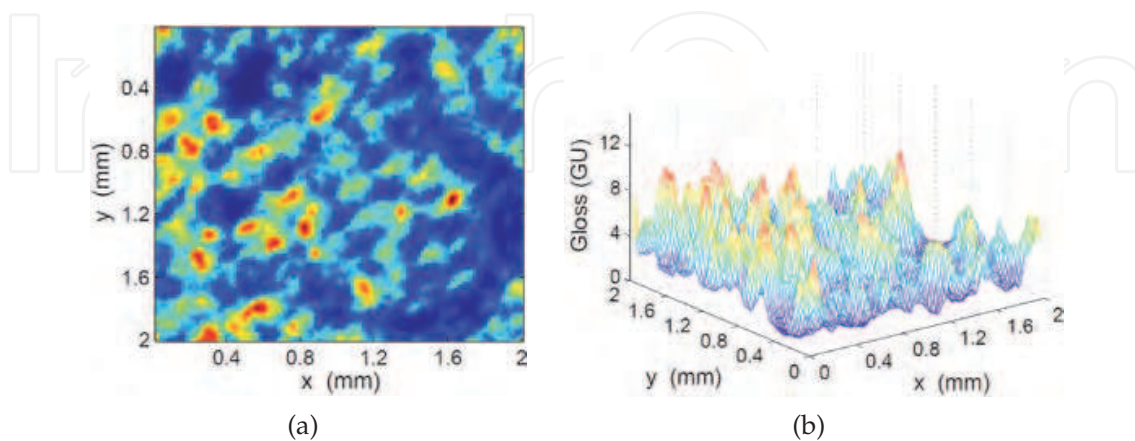


Fig. 4. Gloss from Ti_p surface measured in air. The gloss from the surface is presented (a) as colormap and (b) as meshmap.

The gloss and R_{opt} values can be calculated (see equations 10-13) from the DOE images recorded during the measurements. This calculation is presented in detail in section 3.2. Correlation coefficient between R_{opt} and gloss is ideally -1, because in general when the surface roughness (R_{opt}) increases the reflectance (and G) decreases. Correlation coefficient between the R_{opt} and G values presented in figures 4 and 5 is -0.798.

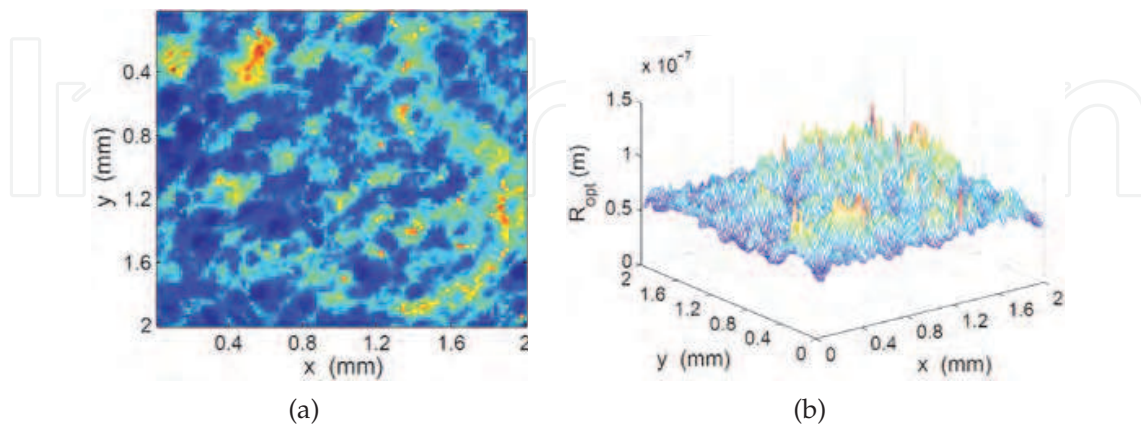


Fig. 5. R_{opt} from Ti_p surface measured in air. The R_{opt} from the surface is presented (a) as colormap and (b) as meshmap.

2.4 AFM and SEM

Atomic force microscopy (AFM) bases on the interaction forces of two materials. When the tip of an AFM is in the proximity of a sample surface, these interaction forces (repulsion and attraction) can be detected by measuring the deviations in laser beam that is reflected from the gold sphere on the cantilever in which the tip is attached. Typically, AFM devices can measure the sample surfaces in contact (tip is touching the surface) and non-contact (tip is floating near the surface) mode. In figure 6a is shown an AFM image from a polished silicon Si(100) surface measured in contact mode.

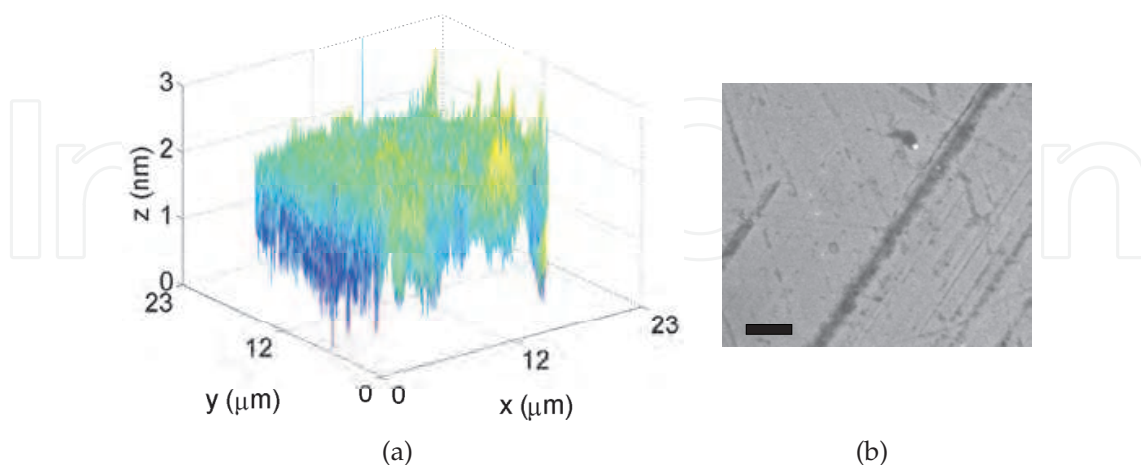


Fig. 6. (a) AFM image from a polished silicon Si(100) wafer surface and (b) SEM image from a Ti_p surface, where the bar denotes distance of $1 \mu\text{m}$.

Scanning electron microscope (SEM) is constructed in such a way that electrons from filament tip are accelerated, focused and deflected (producing scanning) by coils which have been

constructed with knowledge in Coulombian and Lorenzian forces. In figure 6b is shown a SEM image from a polished titanium (Ti_p) surface.

2.5 Spectrophotometry

In spectrophotometry the sample transmittance is measured as a function of wavelength. Thus, the spectrophotometer device includes two equal light pathways for the sample and reference. The probing light is produced from light source like deuterium (UV) and halogen (NIR,VIS) and monochromatized and detected separately with 1 kHz rate for both light paths with a detector (typically one for the UV and one for the VIS/NIR/IR/FIR wavelength regions). Typical parameters, which can be measured by spectrophotometers, are spectral transmittance ($T(\lambda)$), reflectance ($R(\lambda)$) and absorbance ($A(\lambda)$) are presented as follows

$$T(\lambda) = \frac{L_{\lambda t}}{L_{\lambda 0}}, \quad (7)$$

$$R(\lambda) = \frac{L_{\lambda r}}{L_{\lambda 0}}, \quad (8)$$

$$A(\lambda) = \log_e \left(\frac{L_{\lambda 0}}{L_{\lambda t}} \right) = \alpha z = \frac{4\pi\kappa}{\lambda} z, \quad (9)$$

where λ is wavelength, $L_{\lambda t}$, $L_{\lambda 0}$ and $L_{\lambda r}$ are the spectral radiance through, incoming and reflected from the surface respectively, α is the absorption coefficient, κ is the extinction coefficient and z is the optical path length in sample. In figure 7 is presented the absorbance of phosphate buffered saline (PBS) and human plasma fibrinogen (HPF) solutions calculated from spectrophotometer measurements.

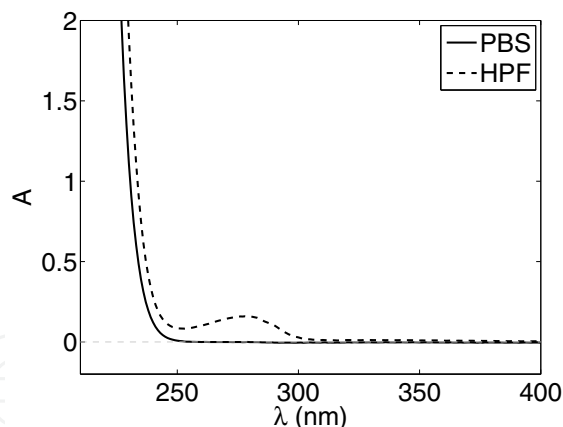


Fig. 7. Calculated absorbance A of (a) PBS and (b) 5 μ M HPF solution from spectrophotometer measurement as a function of wavelength λ in nanometers. Optical path length was in solution 10 mm. Black dashed line is the zero absorbance baseline.

3. Sensing of protein molecules

3.1 VASE sensing of protein adsorption

With equation 9 (Beer-Lambert law) one can calculate, from ellipsometry data, the thickness of layer on a sample surface. This requires a smooth sample surface on which the layer (i.e. the proteins) exists. When considering the layer thickness, the sample surfaces complex refractive index without the layer must be measured first and thereafter the measurements are repeated

when the layer exists on the sample surface. Then, knowing the complex refractive index N of the formed layer, one can solve the z (double of the layer thickness) from equation 9. As the ellipsometry measurements are done in air, measurements of protein layers should be performed as fast as possible (at least within half an hour), because the drying could have denaturing effects on the proteins.

3.2 Coherent and noncoherent response of DOE sensor

The analysis of DOE image consist of calculating the non-coherent, equation 10, and coherent, equation 11, part of the optical signal, which relate to permittivity and optical roughness, respectively as follows (Silvennoinen, Peiponen & Myller, 2008)

$$I_{NC} = \frac{1}{n_{SW}m_{SW}} \sum_{i_{SW}=1}^{n_{SW}} \sum_{j_{SW}=1}^{m_{SW}} I_{i_{SW},j_{SW}} - I_C, \quad (10)$$

where I_C is the coherent portion of the optical signal being

$$I_C = \frac{1}{n_{pk}m_{pk}} \sum_{i_{pk}=1}^{n_{pk}} \sum_{j_{pk}=1}^{m_{pk}} I_{i_{pk},j_{pk}}. \quad (11)$$

In equations 10 and 11 $I_{i,j}$ denotes the irradiance of reflected probe beam, n_{SW} and m_{SW} are the total numbers of sensor pixel dimensions in signal window (SW), n_{pk} and m_{pk} denotes the respective pixel dimension of each of the 16 peaks (pk) in the DOE image. Gloss G measured in gloss units (GU) is standard measure for optical characterization of a surface. Gloss is a function of three different variables: permittivity (ϵ , connected to N), angle of incidence (θ_i) and topography (roughness). Gloss values are calculated from the DOE image when the coherent response, the CCD values of the peaks, is removed from the CCD values of the DOE image (equation 10). DOE image is produced from the irradiance of the reflected probe beam and because of that, this calculation removes the phase information from this beam, leaving the information (I_{NC}) of the surface reflectance and thus ϵ and N . The calculated I_{NC} for the surface (I_{NCs}) values are normalized with the non-coherent response from black glass I_{NCr} , resulting the gloss value to be as follows

$$G = \frac{I_{NCs}}{I_{NCr}} \times 100. \quad (12)$$

In turn, the optical roughness (R_{opt}) values can be calculated from the DOE image utilizing the equation 11. The I_C values contain the phase information of the reflected probe beam. When the probe light beam is reflected from rough surface, the initial coherence degree of the wave front decreases and distortion appears in DOE image 4×4 peaks (I_C values). Finally, the optical roughness R_{opt} values can be calculated from the following equation

$$R_{opt} = \sqrt{-\log_e \left(\frac{1 - R_s}{1 - R_r} \frac{I_{Cs}}{I_{Cr}} \right)} \frac{\lambda}{4\pi}, \quad (13)$$

where R is reflectance calculated from complex refractive index (N) values measured by variable angle spectro-ellipsometer (VASE), λ is the wave length of the probe beam, and the subscripts s and r denote sample and reference respectively. R_{opt} changes of the investigated surfaces can be determined with accuracy of 0.2 nm (in liquid), which is the detection limit of this one-arm interferometer and reasonable sensitivity to detect nanoscale changes appearing in the bioenvironments (Silvennoinen, Hason, Vetterl, Penttinen, Silvennoinen,

Myller, Cernochova, Bartakova, Prachar & Cvrcek, 2010; Silvennoinen, Peiponen & Myller, 2008; Silvennoinen, Vetterl, Hason, Tuononen, Silvennoinen, Myller, Cvrcek, Vanek & Prachar, 2008).

3.3 DOE sensing of protein adsorption

DOE protein detection was performed by placing the surface vertically in a cuvette in order to minimize the effect of sedimentation. The background electrolyte was phosphate buffered saline (PBS, pH ~ 7.4) prepared with 8 mM Na_2HPO_4 , 1.8 mM KH_2PO_4 , 140 mM NaCl, and 2.7 mM KCl with the addition of 136 mM sodium citrate. HPF (fraction I, type III) was purchased from Sigma. Optical analysis was done with a 500 nM HPF solution at room temperature. After filling the sample cuvette with water, the baseline measurement for each sample were performed. After the baseline measurement in water, either the background electrolyte or the protein solution was injected in the cuvette.

Human plasma fibrinogen (HPF), found in the circulatory system at a concentration of 2.6 mg/ml is the key structural glycoprotein in blood clotting which, upon thrombin activation, self-assembles forming a fibrin clot. Having a mass of 340 kDa, the rod-like molecule, 46 nm long is a genuine covalent dimer, the two halves having identical sequences that are linked by a central globular domain. Each monomer has three non-identical chains, $A\alpha$, $B\beta$, and γ connected together at the N-terminus by 11 disulfide bridges forming the 'disulfide knot'. The C-terminus of each chain is globular. Those of the α and γ chains extend forming dumbbell shaped ends to the molecule termed the 'D' regions, while the $A\alpha$ chain globular domains, termed the αC units, interact with each other at the central 'E' region (Wasilewska et al., 2009). Firstly, we study the adsorption ability of HPF proteins on mechanically polished titanium surface by diffractive optical element based sensor (dynamical measurement of adsorption process of protein on surface in electrolyte solution - wet measurement) and ellipsometry (measurement of thickness of adsorbed protein layer on titanium surface after removal the protein-modified surface from protein solution followed by half hour drying in air-dry measurement).

In figure 8 is presented the calculated effects to light reflectance from additional layer (X), PBS electrolyte, air or oxides, on the used polished titanium surface (Ti_p) (figure 8a) and alloy surfaces (figure 8b).

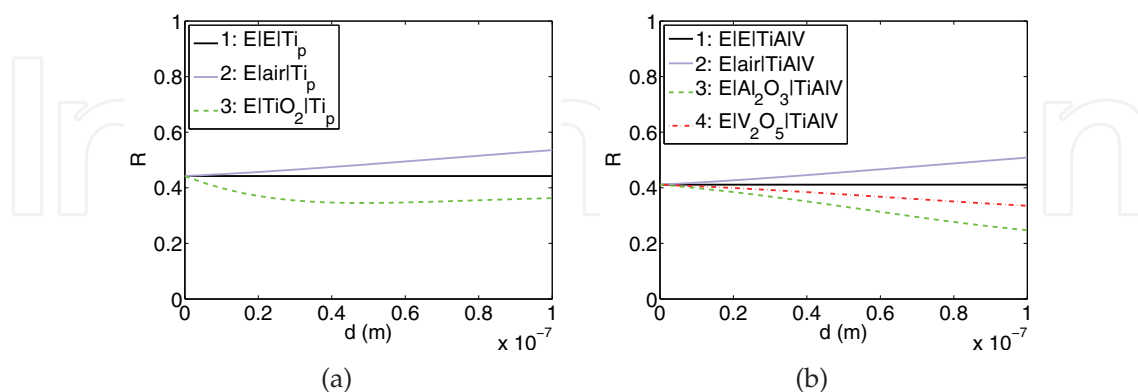


Fig. 8. Calculated reflectance R as a function of layer thickness d on (a) Ti_p and (b) $\text{Ti}_6\text{Al}_4\text{V}$ surfaces ($\lambda = 632.8$ nm). In legend E denotes electrolyte and format $E|X|\text{Ti}$ denotes the material layer X between electrolyte and titanium. Complex refractive index for the alloy $\text{Ti}_6\text{Al}_4\text{V}$ was measured with VASE and other refractive indexes were taken from the book of Palik (1998).

When effective air layer appears on the surface, the reflectance increases. This air layer exists on the surface in liquid in the form of nanobubbles. On the contrary the formation of oxide layer on the surface, for the calculated oxides TiO_2 , Al_2O_3 and V_2O_5 decreases the reflectance, and thus the observed gloss values.

Figure 9 presents the temporal responses of gloss and R_{opt} from a polished titanium surface (Ti_p) surface when surface is immersed in water and in PBS without and with HPF molecules.

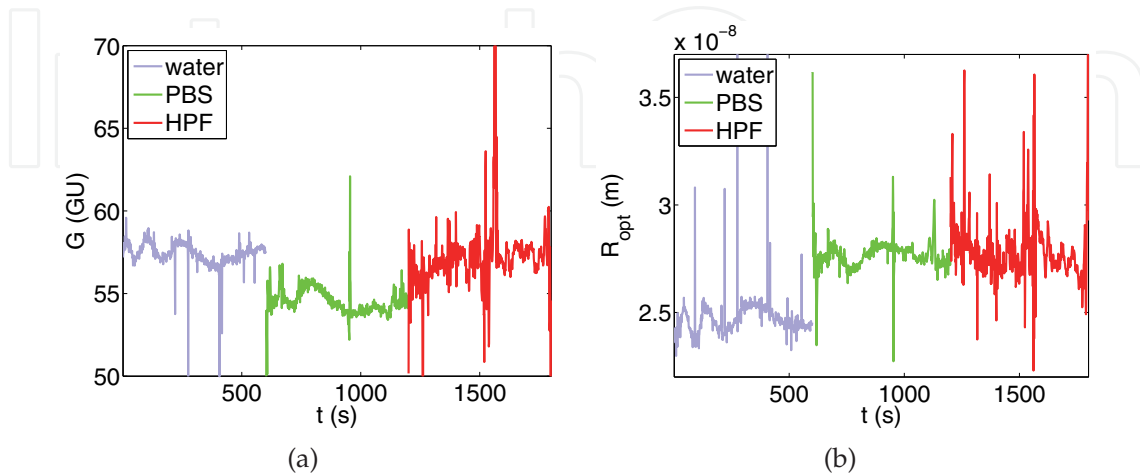


Fig. 9. (a) Temporal gloss (G) in GU and (b) optical roughness R_{opt} in meters of a Ti_p surface, when the surface is in water, in PBS without and with HPF-molecules with 500 nM concentration.

When the surface is presented with the PBS, gloss decreases and R_{opt} increases. This is caused by the chemical reaction from PBS, causing surface energy driven formation of oxides and the mobility of initial gas nanobubbles on the surface (see figure 8). Also the formation of additional nanobubbles can occur, but that would require increase in gloss values, like observed in similar case with Ti6Al4V surface in figure 10.

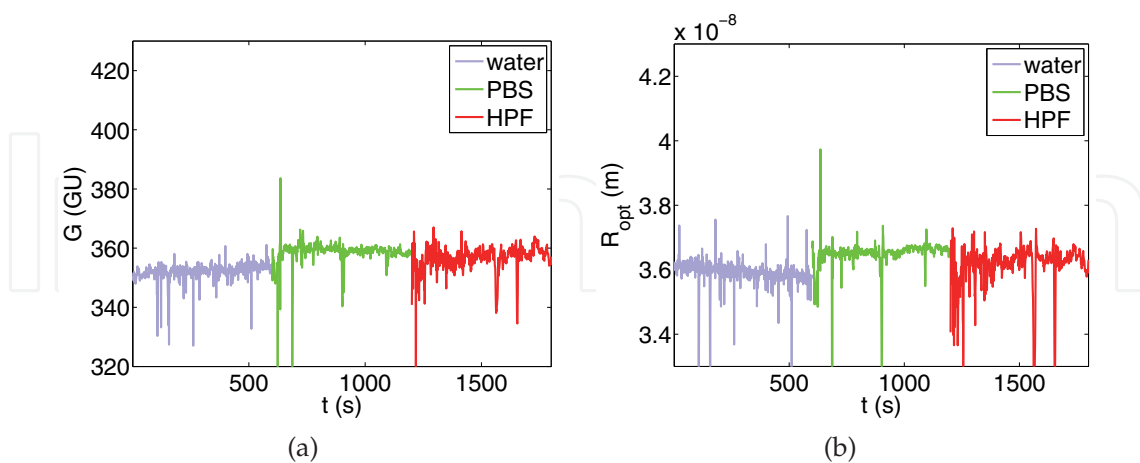


Fig. 10. (a) Temporal gloss (G) in GU and (b) optical roughness R_{opt} in meters of a Ti6Al4V surface, when the surface is in water, in PBS without and with HPF-molecules with 500 nM concentration.

After the PBS solution measurement the cuvette is emptied and the HPF solution is injected in the cuvette. The HPF solution typically has higher changes in the signal from water than

the PBS, which in turn indicates that the proteins are attaching on the surface. Because of the initial reactions with the PBS solution, the changes that are observed, are the change of gloss and R_{opt} values from water baseline to HPF solution. From the temporal responses of Ti_p and $Ti6Al4V$ like presented in figures 9 and 10 can be noted the stronger reaction of Ti_p compared to the $Ti6Al4V$, which seems more inert in observed gloss and R_{opt} changes than Ti_p .

3.4 Effect of titanium surface treatment on protein adsorption

In figures 11 and 12 are presented the average values from measurement involving a polished titanium surface (Ti_p) and $Ti6Al4V$ surfaces. All surfaces indicates an initial reaction with the PBS as the gloss decreases, when the PBS without the HPF molecules is injected in the sample cuvette. This is caused by the formation of oxides on the surfaces (see figure 8). At the same time the R_{opt} values have different trends. In the case of the $Ti6Al4V$ alloy, the R_{opt} mean values are higher with the PBS than with the water on surfaces, but on the other hand in the case of titanium, PBS average R_{opt} value is lower compared to the water. This kind of changes in R_{opt} values can be caused by two main reactions of the PBS (i) the mobility of nanobubbles on the surface and additional formation of them and (ii) the surface energy driven formation of oxides. Additional formation of nanobubbles would be seen as an increase in the mean values of the gloss, as the effective layer formed by the bubbles on the surfaces would increase the surface reflection and thus the gloss. However this is not the case observed in the values of the Ti_p and $Ti6Al4V$ surfaces.

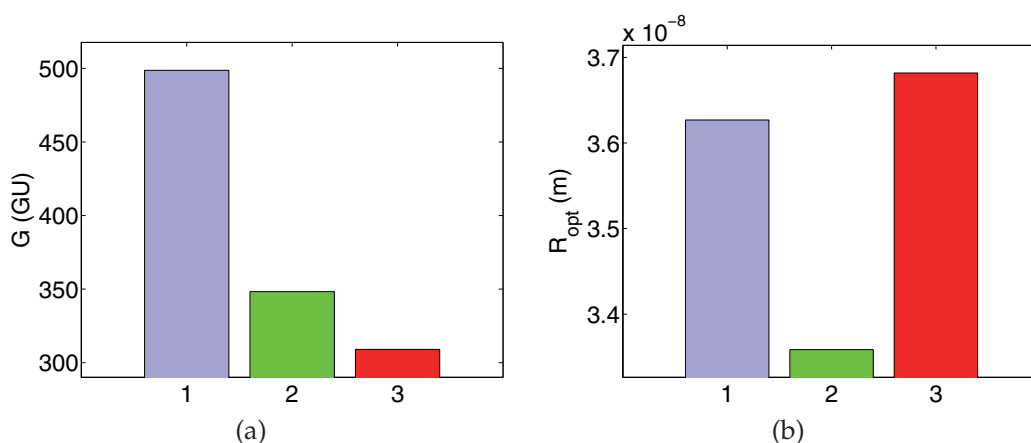


Fig. 11. Average G in GU and optical roughness (R_{opt}) in meters for Ti_p surface. (1) denotes the values from water (2) from PBS and (3) from HPF solution covered surfaces.

When the PBS without the protein is removed, the HPF solution (PBS based) is injected in the sample cuvette. The average signal levels from the HPF measurement are denoted with (3) in the figures 11 and 12. All surfaces indicate lower gloss and higher R_{opt} values than in water, as the proteins are attached on the surface. Also, when comparing the signal value changes from PBS to HPF solution, the changes are similar, which furthermore supports the interpretation that the proteins are attached to the surface. HPF solution is essentially PBS solution with added proteins and when measuring all three types of liquids, in order water, PBS and HPF, one can see the magnitude difference of the adhesion process of samples with DOE sensor data.

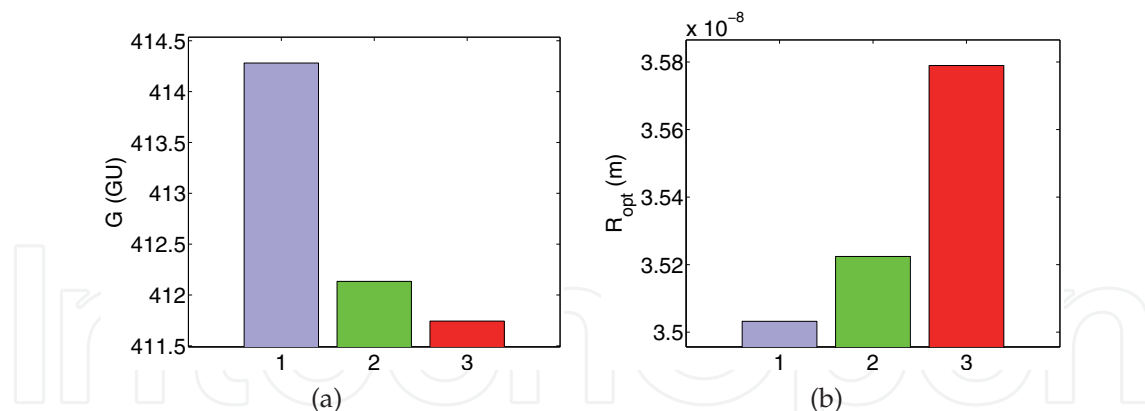


Fig. 12. Average G in GU and optical roughness (R_{opt}) in meters for Ti6Al4V surface. (1) denotes the values from water (2) from PBS and (3) from HPF solution covered surfaces.

As the titanium surface Ti_p is known surface for good biocompatibility, the results (gloss and R_{opt} values) are compared to it. When comparing the results from Ti_p and Ti6Al4V surfaces, one can see that the Ti6Al4V samples are not presenting changes as big as the Ti_p . This would indicate that the Ti6Al4V is not so active as adhesive surface as Ti_p is. The Ti6Al4V behaves in this measurement like an inert surface i.e. indicating unfavorable attachment properties for the HPF molecule.

3.5 Effect of aging of titanium surface on protein adsorption

Effects of aging of the biosurfaces has been studied for titanium-doped hydrocarbon by Silvenoinen, Vetterl, Hason, Tuononen, Silvenoinen, Myller, Cvrcek, Vanek & Prachar (2008). In this study the aging process was observed in 2 years time and the results showed that the long time storage causes impurities to the original surfaces. These impurities was interpreted to be caused by the molecules in air including the carbon and the oxygen. Results showed that the initial adsorption abilities of the measured surfaces were greatly decreased by the long time storage. Thus the aging of biosurface, which have properties to form oxides and other chemical bonds in low energies, should be always considered. For example we measured complex refractive indexes ($\lambda = 632.8\text{nm}$) of polished titanium Ti_p and stored titanium Ti_{sto} in aim to compare the possible changes on the surface properties. Complex refractive indexes were $N(Ti_p) = 2.616 + 2.413i$ and $N(Ti_{sto}) = 2.002 + 2.077i$ and respective reflectances were $R(Ti_p) = 0.446$ and $R(Ti_{sto}) = 0.399$. If oxidation of the surface is assumed to be the only reaction on these titanium surfaces, we can estimate from figure 8a the layer thickness of formed native titanium dioxide on this stored surface to be ca. 10 nm. This already would impact on the adhesive properties of the titanium.

4. Alternative optical testing of biocompatibility

4.1 Biological methods in determining the biocompatibility

Cytocompatibility as a basis for biocompatibility testings for several titanium β -alloys (β structure is body-centered cubic structure) has been investigated for example by Bartakova et al. (2009). In this study the possible usage of titanium alloys in dental implants was studied *in-vitro* environment by means of three different tests from which one can determine the biological acceptance of certain material. Test of the cell-spread on standard substrate (coverglass or bottom of culture flask) with (1) inoculation and (2) cell monolayer (both tests used time-lapse capturing of pictures) and (3) assay tests showing possible chromosome

aberrations, mutagenesis and neoplastic cell forming. Differences for methods (1) and (2) is that in (1) the cells are inoculated on the surface having lower cell density than in (2) in which the cell density is around 70 %. The results are evaluated by optically or with scanning electron microscopy which can show morphological anomalies on cell membrane surface.

4.2 Cytocompatibility of dental implants alloys

In cell area dilatation test (spreading test) it is possible to use any heteronuclear cell line, for example HeLa, L929, PtK, CHO and other. Aim of this test is to show time for full spreading (dilatation) on standard substrate. Standard substrate is a coverglass, or bottom of culture flask. Positive control is a laboratory standard, negative control is a glass surface or inner surface of culture flask.

Experiment shows an ability of cell membrane to spread and evaluates some disturbance in a cell attached mechanisms on the surface. When the environment is a toxic matter, the cell area dilatation (spreading) is very low and this is a marker for damage of cell membranes. When cells didn't spread, the material was interpreted to be toxic. Zone between 50 and 70 % of cell spread is kept tolerant and 80 and 99 % is interpreted as a cytocompatible material when cultivation time is kept constant. Example of light microscope image of cell area dilation tests shown in figures 13 and 14 for Ta and Cu surfaces respectively.

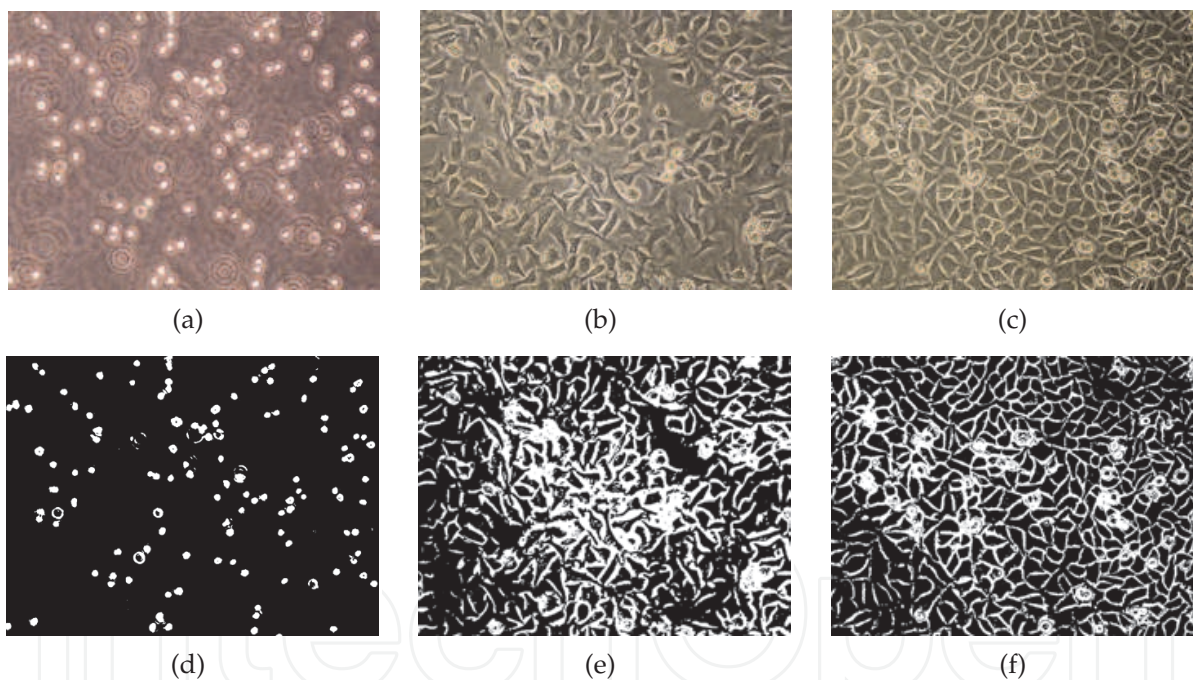


Fig. 13. Evolution of cell spread on Ta surface. Light microscope images from the surface after (a,d) 0 min, (b,e) 120 min and (c,f) 500 min of inoculation. (d), (e) and (f) shows the corresponding processed images.

To make the area occupied by the cells more visible, we have processed the optical microscope images (see figures 13 and 14) by chroma tone threshold processing.

From figures 13 and 14 one can observe the difference of higher (figure 13) and lower (figure 14) cell area dilation. Higher cell division rate on Ta surface indicates that the surface can hold cells on it while the cells maintain their natural division abilities, thus the Ta surface could be considered as a cytocompatible surface. The Cu surface shows toxic reaction to the cells (see figure 14) as the cells are not propagating on the surface and some of the cells shows lost

of their biological function. From the images b and c in the figure 14, the dying cells can be observed to have black nucleus from the consequence of increased light absorption of lost cell chromosomes.

Optical analysis of Ti_p and Ti6Al4V from the gloss and R_{opt} data in the section 3.4 indicated that the Ti6Al4V surface is not showing strong reaction in the HPF adsorption, but polished titanium surface (Ti_p) is observed to adsorb the HPF molecules. In the study by Bartakova et al. (2009), the Ti6Al4V alloy was recognized to be biologically tolerant, but not as good as Ti_p (biocompatible), thus the two studies seem to be consistent with each other.

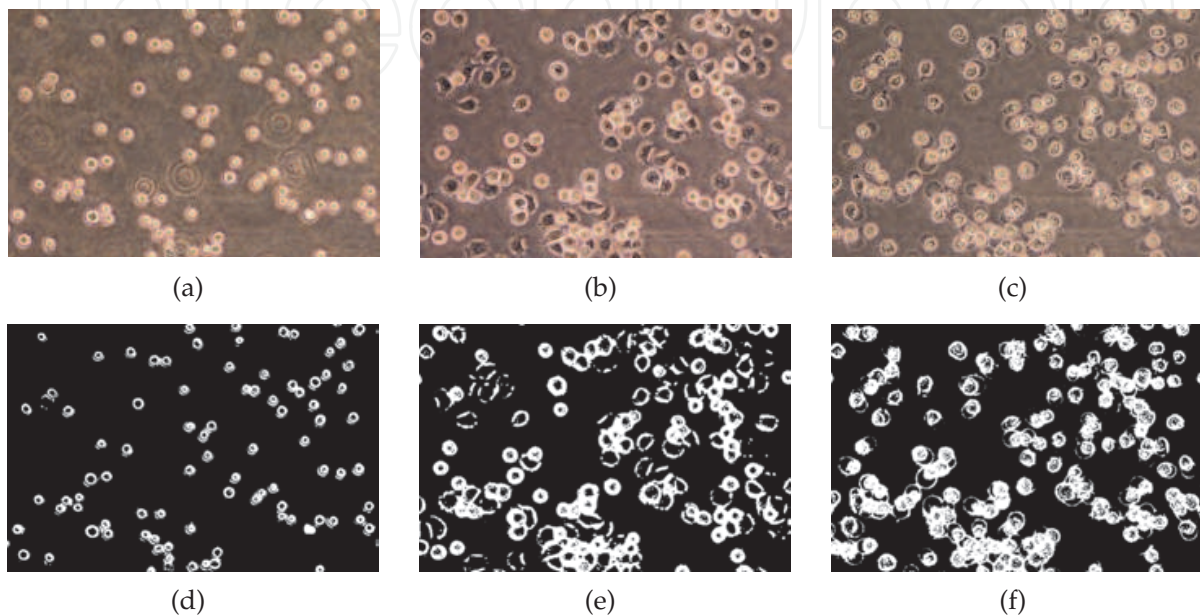


Fig. 14. Evolution of cell spread on Cu surface. Light microscope images from the surface after (a,d) 0 min, (b,e) 40 min and (c,f) 180 min of inoculation. (d), (e) and (f) shows the corresponding processed images.

5. Conclusion

Doped titanium alloys can show both mechanical and biocompatibility properties that exceed the ones of titanium, which has been the often used biomaterial in bioapplications. Study results reported here indicated that many dopant for titanium can be used, but the initial biological reaction should be observed before using the doped titanium in applications. Before the optical detection the surface needs to be characterized. The characterization of the surface is not only basis for the optical measurement, but also helps one to understand more about the biophysical reactions that occurs with the biomolecules on the surface. Results presented here shows that optical detection of biomolecules is a capable non-contact method for determining the reaction of the biomolecules on a surface *in-vitro*. Especially the diffractive optics based elements as the DOE, which can measure multiple surface parameters simultaneously, could give promising new aspects in development of future bio-optoelectronics.

6. Acknowledgement

This work was supported by the Grant Agency of the Czech Republic (P205/10/2378) and the Academy of Sciences of the Czech Republic (KAN200040651), the Ministry of

Education, Youth and Sport of the Czech Republic (1M0528), and institutional research plans (AVOZ50040507 and AVOZ50040702) and the Academy of Finland (131539/31.03.2009).

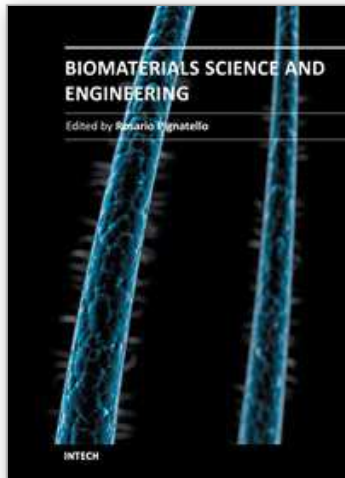
7. References

- Agnihotri, A. & Siedlecki, C. (2004). Time-dependent conformational changes in fibrinogen measured by atomic force microscopy, *Langmuir* 20(20): 8846–8852.
- Archana, P., Jose, R., Jin, T., Vijila, C., Yusoff, M. & Ramakrishna, S. (2010). Structural and electrical properties of nb-doped anatase TiO₂ nanowires by electrospinning, *Journal of The American Ceramic Society* 93(12): 4096–4102.
- Ball, V., Bentaleb, A., Hemmerle, J., Voegel, J. & Schaaf, P. (1996). Dynamic aspects of protein adsorption onto titanium surfaces: Mechanism of desorption into buffer and release in the presence of proteins in the bulk, *Langmuir* 12(6): 1614–1621.
- Barajas-Ledesma, E., Garcia-Benjume, M., Espitia-Cabrera, I., Bravo-Patino, A., Espinoza-Beltran, F., Mostaghimi, J. & Contreras-Garcia, M. (2010). Photocatalytic activity of Al₂O₃-doped TiO₂ thin films activated with visible light on the bacteria *escherichia coli*, *Materials Science and Engineering B* 174(1-3, Sp. Iss. SI): 74–79.
- Bartakova, S., Prachar, P., Kudrman, J., Brezina, V., Podhorna, B., Cernochova, P., Vanek, J. & Strecha, J. (2009). New titanium beta-alloys for dental implantology and their laboratory-based assays of biocompatibility, *Scripta Medica* 82(2): 76–82.
- Brett, P., Harle, J., Salih, V., Mihoc, R., Olsen, I., Jones, F. & Tonetti, M. (2004). Roughness response genes in osteoblasts, *Bone* 35(1): 124–133.
- Cacciafesta, P., Hallam, K., Watkinson, A., Allen, G., Miles, M. & Jandt, K. (2001). Visualisation of human plasma fibrinogen adsorbed on titanium implant surfaces with different roughness, *Surface Science* 491(3): 405–420.
- Cacciafesta, P., Humphris, A., Jandt, K. & Miles, M. (2000). Human plasma fibrinogen adsorption on ultraflat titanium oxide surfaces studied with atomic force titanium oxide surfaces studied with atomic force, *Langmuir* 16(21): 8167–8175.
- Cai, K., Bossert, J. & Jandt, K. (2006). Does the nanometre scale topography of titanium influence protein adsorption and cell proliferation?, *Colloids and Surfaces B-biointerfaces* 49(2): 136–144.
- Cai, K., Muller, M., Bossert, J., Rechtenbach, A. & Jandt, K. (2005). Surface structure and composition of flat titanium thin films as a function of film thickness and evaporation rate, *Applied Surface Science* 250(1-4): 252–267.
- Cantau, C., Pigot, T., Dupin, J. & Lacombe, S. (2010). N-doped TiO₂ by low temperature synthesis: Stability, photo-reactivity and singlet oxygen formation in the visible range, *Journal of Photochemistry and Photobiology A-chemistry* 216(2-3, Sp. Iss. SI): 201–208.
- Choi, J., Park, H. & Hoffmann, M. (2010). Combinatorial doping of TiO₂ with platinum (Pt), chromium (Cr), vanadium (V), and nickel (Ni) to achieve enhanced photocatalytic activity with visible light irradiation, *Journal of Materials Research* 25(1, Sp. Iss. SI): 149–158.
- Choukourov, A., Grinevich, A., Slavinska, D., Biederman, H., Saito, N. & Takai, O. (2008). Scanning probe microscopy for the analysis of composite ti/hydrocarbon plasma polymer thin films, *Surface Science* 602(5): 1011 – 1019.
- Cochran, D. (1999). A comparison of endosseous dental implant surfaces, *Journal of Periodontology* 70(12): 1523–1539.
- Czoska, A., Livraghi, S., Paganini, M., Giamello, E., Di Valentin, C. & Pacchioni, G. (2011). The nitrogen-boron paramagnetic center in visible light sensitized N-B Co-doped TiO₂.

- experimental and theoretical characterization, *Physical Chemistry Chemical Physics* 13(1): 136–143.
- Darriba, G., Errico, L., Eversheim, P., Fabricius, G. & Renteria, M. (2009). First-principles and time-differential gamma-gamma perturbed-angular-correlation spectroscopy study of structural and electronic properties of Ta-doped TiO₂ semiconductor, *Physical Review* 79(11).
- Galli, C., Coen, M., Hauert, R., Katanaev, V., Wymann, M., Groning, P. & Schlapbach, L. (2001). Protein adsorption on topographically nanostructured titanium, *Surface Science* 474(1-3): L180–L184.
- Garguilo, J., Davis, B., Buddie, M., Kock, F. & Nemanich, R. (2004). Fibrinogen adsorption onto microwave plasma chemical vapor deposited diamond films, *Diamond and Related Materials* 13(4-8): 595–599.
- Grinevich, A., Bacakova, L., Choukourov, A., Boldyryeva, H., Pihosh, Y., Slavinska, D., Noskova, L., Skuciova, M., Lisa, V. & Biedermanl, H. (2009). Nanocomposite ti/hydrocarbon plasma polymer films from reactive magnetron sputtering as growth support for osteoblast-like and endothelial cells, *Journal of Biomedical Materials Research Part A* 88(4): 952–966.
- Hemmersam, A., Foss, M., Chevallier, J. & Besenbacher, F. (2005). Adsorption of fibrinogen on tantalum oxide, titanium oxide and gold studied by the QCM-D technique, *Colloids and Surfaces B-biointerfaces* 43(3-4): 208–215.
- Höök, F., Vörös, J., Rodahl, M., Kurrat, R., Boni, P., Ramsden, J., Textor, M., Spencer, N., Tengvall, P., Gold, J. & Kasemo, B. (2002a). A comparative study of protein adsorption on titanium oxide surfaces using in situ ellipsometry, optical waveguide lightmode spectroscopy, and quartz crystal microbalance/dissipation, *Colloids and Surfaces B-biointerfaces* 24(2): 155–170.
- Höök, F., Vörös, J., Rodahl, M., Kurrat, R., Böni, P., Ramsden, J., Textor, M., Spencer, N., Tengvall, P., Gold, J. & Kasemo, B. (2002b). A comparative study of protein adsorption on titanium oxide surfaces using in situ ellipsometry, optical waveguide lightmode spectroscopy, and quartz crystal microbalance/dissipation, *Colloids and Surfaces B: Biointerfaces* 24(2): 155–170.
- Huang, L., Ning, C., Ding, D., Bai, S., Qin, R., Li, M. & Mao, D. (2010). Wettability and in vitro bioactivity of doped TiO₂ nanotubes, *Journal of Inorganic Materials* 25(7): 775–779.
- Huang, N., Yang, P., Leng, Y., Chen, J., Sun, H., Wang, J., Wang, G., Ding, P., Xi, T. & Leng, Y. (2003). Hemocompatibility of titanium oxide films, *Biomaterials* 24(13): 2177–2187.
- Imamura, K., Shimomura, M., Nagai, S., Akamatsu, M. & Nakanishi, K. (2008). Adsorption characteristics of various proteins to a titanium surface, *Journal of Bioscience and Bioengineering* 106(3): 273–278.
- Jackson, D., Omanovic, S. & Roscoe, S. (2000). Electrochemical studies of the adsorption behavior of serum proteins on titanium, *Langmuir* 16(12): 5449–5457.
- Jandt, K. (2001). Atomic force microscopy of biomaterials surfaces and interfaces, *Surface Science* 491(3): 303–332.
- Jansson, E. & Tengvall, P. (2004). Adsorption of albumin and IgG to porous and smooth titanium, *Colloids and Surfaces B-biointerfaces* 35(1): 45–51.
- Jones, M., Mccoll, I., Grant, D., Parker, K. & Parker, T. (2000). Protein adsorption and platelet attachment and activation, on TiN, TiC, and DLC coatings on titanium for cardiovascular applications, *Journal of Biomedical Materials Research* 52(2): 413–421.

- Khaleel, A., Shehadi, I. & Al-shamisi, M. (2010). Structural and textural characterization of sol-gel prepared nanoscale titanium-chromium mixed oxides, *Journal of Non-crystalline Solids* 356(25-27): 1282–1287.
- Kidoaki, S. & Matsuda, T. (1999). Adhesion forces of the blood plasma proteins on self-assembled monolayer surfaces of alkanethiolates with different functional groups measured by an atomic force microscope, *Langmuir* 15(22): 7639–7646.
- Ma, W., Ruys, A., Mason, R., Martin, P., Bendavid, A., Liu, Z., Ionescu, M. & Zreiqat, H. (2007). DLC coatings: Effects of physical and chemical properties on biological response, *Biomaterials* 28(9): 1620–1628.
- Martin, E., Manceur, A., Polizu, S., Savadogo, O., Wu, M. & Yahia, L. (2006). Corrosion behaviour of a beta-titanium alloy, *Bio-medical Materials and Engineering* 16(3): 171–182.
- Nygren, H., Tengvall, P. & Lundstrom, I. (1997). The initial reactions of TiO₂ with blood, *Journal of Biomedical Materials Research* 34(4): 487–492.
- Palik, E. (1998). *Handbook of Optical Constants of Solids (Volumes I, II and III)*, Academic Press.
- Parsegian, V. (2005). *Van der Waals Forces: A Handbook for Biologists, Chemists, Engineers, and Physicists*, Cambridge University Press, Cambridge.
- Roach, P., Farrar, D. & Perry, C. (2005). Interpretation of protein adsorption: Surface-induced conformational changes, *Journal of the American Chemical Society* 127(22): 8168–8173.
- Roach, P., Farrar, D. & Perry, C. (2006). Surface tailoring for controlled protein adsorption: Effect of topography at the nanometer scale and chemistry, *Journal of the American Chemical Society* 128(12): 3939–3945.
- Roach, P., Shirtcliffe, N., Farrar, D. & Perry, C. (2006). Quantification of surface-bound proteins by fluorometric assay: Comparison with quartz crystal microbalance and amido black assay, *Journal of Physical Chemistry B* 110(41): 20572–20579.
- Rouahi, M., Champion, E., Gallet, O., Jada, A. & Anselme, K. (2006). Physico-chemical characteristics and protein adsorption potential of hydroxyapatite particles: Influence on in vitro biocompatibility of ceramics after sintering, *Colloids and Surfaces B-biointerfaces* 47(1): 10–19.
- Shaama, F. (2005). An in vitro comparison of implant materials cell attachment, cytokine and osteocalcin production, *West Indian Medical Journal* 54(4): 250–256.
- Silvennoinen, R., Hason, S., Vetterl, V., Penttinen, N., Silvennoinen, M., Myller, K., Cernochova, P., Bartakova, S., Prachar, P. & Cvrcek, L. (2010). Diffractive-optics-based sensor as a tool for detection of biocompatibility of titanium and titanium-doped hydrocarbon samples, *Applied Optics* 49(29): 5583–5591.
- Silvennoinen, R., Peiponen, K.-E. & Myller, K. (2008). *Specular gloss*, Elsevier, Amsterdam.
- Silvennoinen, R., Vetterl, V., Hason, S., Silvennoinen, M., Myller, K., Vanek, J. & Cvrcek, L. (2010). Optical sensing of attached fibrinogen on carbon doped titanium surfaces, *Advances in Optical Technologies* 2010(22): 7.
- Silvennoinen, R., Vetterl, V., Hason, S., Tuononen, H., Silvennoinen, M., Myller, K., Cvrcek, L., Vanek, J. & Prachar, P. (2008). Sensing of human plasma fibrinogen on polished, chemically etched and carbon treated titanium surfaces by diffractive optical element based sensor, *Optics Express* 16(14): 10130–10140.
- Soman, P., Rice, Z. & Siedlecki, C. (2008). Measuring the time-dependent functional activity of adsorbed fibrinogen by atomic force microscopy, *Langmuir* 24(16): 8801–8806.
- Sonesson, A., Callisen, T., Brismar, H. & Elofsson, U. (2007). A comparison between dual polarization interferometry (DPI) and surface plasmon resonance (SPR) for protein adsorption studies, *Colloids and Surfaces B-Biointerfaces* 54(2): 236–240.

- Swann, M., Peel, L., Carrington, S. & Freeman, N. (2004). Dual-polarization interferometry: an analytical technique to measure changes in protein structure in real time, to determine the stoichiometry of binding events, and to differentiate between specific and nonspecific interactions, *Analytical Biochemistry* 329(2): 190–198.
- Toscano, A. & Santore, M. (2006). Fibrinogen adsorption on three silica-based surfaces: Conformation and kinetics, *Langmuir* 22(6): 2588–2597.
- Van De Keere, I., Willaert, R., Hubin, A. & Vereeckent, J. (2008). Interaction of human plasma fibrinogen with commercially pure titanium as studied with atomic force microscopy and x-ray photoelectron spectroscopy, *Langmuir* 24(5): 1844–1852.
- Vanderah, D., La, H., Naff, J., Silin, V. & Rubinson, K. (2004). Control of protein adsorption: Molecular level structural and spatial variables, *Journal of the American Chemical Society* 126(42): 13639–13641.
- Walivaara, B., Aronsson, B., Rodahl, M., Lausmaa, J. & Tengvall, P. (1994). Titanium with different oxides - *in-vitro* studies of protein adsorption and contact activation, *Biomaterials* 15(10): 827–834.
- Wang, X., Yu, L., Li, C., Zhang, F., Zheng, Z. & Liu, X. (2003). Competitive adsorption behavior of human serum albumin and fibrinogen on titanium oxide films coated on LTI-carbon by IBED, *Colloids and Surfaces B-biointerfaces* 30(1-2): 111–121.
- Wasilewska, M., Adamczyk, Z. & Jachimska, B. (2009). Structure of fibrinogen in electrolyte solutions derived from dynamic light scattering (DLS) and viscosity measurements, *Langmuir* 25(6): 3698–3704.
- Webster, T., Siegel, R. & Bizios, R. (1999). Osteoblast adhesion on nanophase ceramics, *Biomaterials* 20(13): 1221–1227.
- Wertz, C. & Santore, M. (1999). Adsorption and relaxation kinetics of albumin and fibrinogen on hydrophobic surfaces: Single-species and competitive behavior, *Langmuir* 15(26): 8884–8894.
- Wertz, C. & Santore, M. (2001). Effect of surface hydrophobicity on adsorption and relaxation kinetics of albumin and fibrinogen: Single-species and competitive behavior, *Langmuir* 17(10): 3006–3016.
- Wertz, C. & Santore, M. (2002). Fibrinogen adsorption on hydrophilic and hydrophobic surfaces: Geometrical and energetic aspects of interfacial relaxations, *Langmuir* 18(3): 706–715.
- Xu, L. & Siedlecki, C. (2007). Effects of surface wettability and contact time on protein adhesion to biomaterial surfaces, *Biomaterial* 28(22): 3273–3283.
- Yang, Y., Cavin, R. & Ong, J. (2003). Protein adsorption on titanium surfaces and their effect on osteoblast attachment, *Journal of Biomedical Materials Research Part A* 67a(1): 344–349.



Biomaterials Science and Engineering

Edited by Prof. Rosario Pignatello

ISBN 978-953-307-609-6

Hard cover, 456 pages

Publisher InTech

Published online 15, September, 2011

Published in print edition September, 2011

These contribution books collect reviews and original articles from eminent experts working in the interdisciplinary arena of biomaterial development and use. From their direct and recent experience, the readers can achieve a wide vision on the new and ongoing potentials of different synthetic and engineered biomaterials. Contributions were not selected based on a direct market or clinical interest, than on results coming from very fundamental studies which have been mainly gathered for this book. This fact will also allow to gain a more general view of what and how the various biomaterials can do and work for, along with the methodologies necessary to design, develop and characterize them, without the restrictions necessarily imposed by industrial or profit concerns. The book collects 22 chapters related to recent researches on new materials, particularly dealing with their potential and different applications in biomedicine and clinics: from tissue engineering to polymeric scaffolds, from bone mimetic products to prostheses, up to strategies to manage their interaction with living cells.

How to reference

In order to correctly reference this scholarly work, feel free to copy and paste the following:

Raimo Silvennoinen, Niko Penttinen, Martti Silvennoinen, Stanislav Hasoň, Vladimír Vetterl, Sonia Bartáková, Patrik Prachár, Jiří Vaněk and Vítězslav Březina (2011). Optical Detection of Protein Adsorption on Doped Titanium Surface, Biomaterials Science and Engineering, Prof. Rosario Pignatello (Ed.), ISBN: 978-953-307-609-6, InTech, Available from: <http://www.intechopen.com/books/biomaterials-science-and-engineering/optical-detection-of-protein-adsorption-on-doped-titanium-surface>

INTECH
open science | open minds

InTech Europe

University Campus STeP Ri
Slavka Krautzeka 83/A
51000 Rijeka, Croatia
Phone: +385 (51) 770 447
Fax: +385 (51) 686 166
www.intechopen.com

InTech China

Unit 405, Office Block, Hotel Equatorial Shanghai
No.65, Yan An Road (West), Shanghai, 200040, China
中国上海市延安西路65号上海国际贵都大饭店办公楼405单元
Phone: +86-21-62489820
Fax: +86-21-62489821

© 2011 The Author(s). Licensee IntechOpen. This chapter is distributed under the terms of the [Creative Commons Attribution-NonCommercial-ShareAlike-3.0 License](https://creativecommons.org/licenses/by-nc-sa/3.0/), which permits use, distribution and reproduction for non-commercial purposes, provided the original is properly cited and derivative works building on this content are distributed under the same license.

IntechOpen

IntechOpen